


# Simplified modeling of electromagnets for dynamic simulation of transient effects for a synchronous electric motor

Florian Bechler<sup>1</sup> | Julius Kesten<sup>2</sup> | Florian Wittemann<sup>3</sup> | Frank Henning<sup>3</sup> |  
Martin Doppelbauer<sup>2</sup> | Peter Eberhard<sup>1</sup> 

<sup>1</sup>Institute of Engineering and Computational Mechanics, University of Stuttgart, Stuttgart, Germany

<sup>2</sup>Institute of Electrical Engineering, Karlsruhe Institute of Technology (KIT), Karlsruhe, Germany

<sup>3</sup>Institute of Vehicle System Technology, Karlsruhe Institute of Technology (KIT), Karlsruhe, Germany

## Correspondence

Prof. Peter Eberhard, Institute of Engineering and Computational Mechanics, University of Stuttgart, Stuttgart, Germany.

Email: [peter.eberhard@itm.uni-stuttgart.de](mailto:peter.eberhard@itm.uni-stuttgart.de)

## Funding information

Ministry of Science, Research, and Arts of the Federal State of Baden-Württemberg: ReMos project 'Effiziente Reluktanzmaschine für emissionsfreie Mobilität ohne seltene Erden'

## Abstract

This study aims to show an approach for the dynamic simulation of a synchronous machine. The magnetic forces in the air gap are calculated efficiently using simplified approaches without neglecting important effects. For the modeling of the magnetic forces, an equivalent magnetic circuit is constructed in which the magnetic saturation and the leakage flux are taken into account and coupled with the electrical circuit at the end. The calculated magnetic forces are then passed to a mechanical model of the motor. Together with a predefinable load torque, the resulting motor rotation and the forces in the bearings are identified. The presented model is then investigated in a small example. This novel approach is intended to provide a method of calculating dynamically the forces transmitted from the shaft to the motor housing and to create the basis for evaluating electric motors for vibrations, noise, and harshness under varying loads and input voltages.

## KEYWORDS

dynamic simulation electromagnet, electromagnet modeling, magnetomotive forces

## 1 | INTRODUCTION

While the permanent magnet-assisted synchronous machine (PMS) can achieve high efficiencies, it is very expensive due to the rare earth magnets used in the rotor, which also limits the high-speed capabilities of these machines.<sup>1,2</sup> Synchronous reluctance machines (SynRM), however, can achieve high maximum speeds and are cheaply manufactured thanks to their simple yet robust rotor design. Due to the lack of rotor excitation in SynRMs, they suffer from poor power factors and low power densities.<sup>3</sup>

The ReMoS project ("Effiziente Reluktanzmaschine für emissionsfreie Mobilität ohne seltene Erden"—reluctance machine for

emission-free mobility without rare earth materials) aims to design a variable-flux magnet-assisted SynRM to combine the high maximum speeds of SynRMs and the high base speed torque of PMSs. The flux barriers are filled with fiber-reinforced polymers to ensure the maximum sturdiness of the rotor and the stator is cooled with internal slot cooling to enable high current densities.<sup>4,5</sup>

AlNiCo magnets are applied to the rotor. They combine high remnant flux densities with small coercive forces, which allow for a change of the magnetization state during operation.<sup>6</sup> Together with the operation in the higher speed range, it is necessary to analyze the vibrations, which the rotor passes on to the housing via the rotor bearings. These investigations are usually carried out with finite element analysis (FEA)<sup>7</sup> focusing on the static force

This is an open access article under the terms of the Creative Commons Attribution License, which permits use, distribution and reproduction in any medium, provided the original work is properly cited.

© 2021 The Authors. *International Journal of Mechanical System Dynamics* published by John Wiley & Sons Australia, Ltd on behalf of Nanjing University of Science and Technology.

characteristics and flux distributions, which is time-consuming and offers limited flexibility for design modifications. Other modeling approaches like the equivalent magnetic circuit (EMC)<sup>8</sup> provide information on static working points only and neglect effects resulting from magnetic saturation, which become significant for higher loads and speeds. The identification of parameters in simplified magnet models based on surrogate parameters is usually a challenging task and these models are often only valid in a small frequency range.

This article discusses the possibilities to model the magnetic forces transiently while taking into consideration the magnetic saturation and leakage flux and transfer the calculated forces into a mechanic model to investigate the forces that occur in the bearings and the housing. In Section 2, the simulation framework is described with the inputs and outputs for each subsystem. In Section 2.1 the modeling of the magnetomotive forces is depicted in detail. The used detailed EMC surrogate model, including magnetic reluctance, leakage flux, magnetic saturation, and fringing is described and the challenging part of transforming the implicit differential equations (IDEs) into a differential algebraic system is explained. Beginning with a flux-based model, taking the mentioned effects into account, the EMC is coupled with the electric circuit which results in a semi-implicit differential equation. The calculated magnetomotive forces are then transferred to the mechanical model, which is described in Section 2.2. Using Neweul-M<sup>2</sup>,<sup>9</sup> the system containing the rotor and the shaft is formulated as a rigid multibody system,<sup>10</sup> with force application points as input and with the mechanical states as output. Afterward, in Section 3, a small example simulation is presented with a user-defined load torque and input voltage. In Section 4, a short conclusion is drawn with respect to the current capabilities of the model and an outlook on how the presented system can be used and improved.

## 2 | MODELING

The motor considered in this study is a three-phase synchronous motor with eight poles, so the stator consists of 48 teeth. The number of slots per pole and phase is  $q = 2$ . In synchronous machines, the spatially distributed windings in the stator are fed by sinusoidally alternating voltages with a phase shift of  $2/3 \pi$  relative to each other. These input voltages cause currents in the winding thus creating a rotating magnetic field. The rotor speed is synchronous to the magnetic field in the stator granting the machine its name. As depicted in Figure 1, the simulation model is divided into two parts. The system input is a voltage  $U_{\text{input}}$ , which is used to calculate the magnetomotive forces in the air gap in the magnetic model. The calculated magnetic forces  $F_{\text{mag rad,tan}}$  are

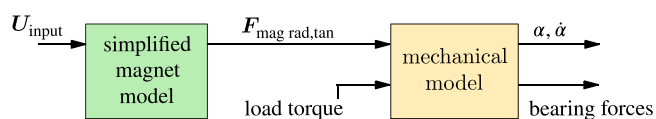


FIGURE 1 Structure of the simulation model

then transferred to the mechanical model, together with user-defined load torque. As a result, the bearing forces, the generated motor torque, and the mechanical states  $\alpha$  and its derivative are calculated. This modular and generic structure allows quick adjustments in the implementation if the motor geometry, number of pole pairs, or inputs are changed.

In Figure 2, the stator with the three-phase windings around the teeth and the rotor are shown. In Ref. 11 a detailed approach of modeling the magnets in a long stator motor is described. The modeling approach of the synchronous motor in this study is quite similar regarding the mathematical formulation and transformation of the differential equation, so details can be found there. In the following, it is only briefly described to convey the underlying idea. Important for the behavior of the magnets are the air gap  $s$  between rotor and stator, the length of the flux lines in the iron  $l_{Fe}$ , the permeability of the iron  $\mu_r$  with its variation by the current  $I$ , and the movement of the flux lines along the stator and rotor. Also, the magnetic hysteresis, the occurring coupling capacities in high frequencies, and the change of the air gap due to an elastic shaft or an eccentricity of the rotor have an influence on the magnetomotive force but are neglected in this simplified approach. The calculated forces of the electromagnetic model are the inputs for the mechanical model. This can be used to calculate, for example, the bearing forces. Note that here a transient dynamic simulation must be done and so methods like the finite element method (FEM) are not feasible due to their enormous computation times.

### 2.1 | Modeling of the magnetic circuit

The idea is to replace the magnetic currents and effects with equivalent electrical currents and components. An extract of the EMC is shown in Figure 2 and is described in the following.

The reluctances  $R_{Fe,St,i}$  and  $R_{Fe,R,i}$  describe the flux per pole along the stator back and the iron rotor. The reluctance  $R_{\sigma,i}$  characterizes the loss across the stator teeth to the next winding and  $R_{L,i}$  the reluctance in the air gap.<sup>11</sup> The magnetic voltage sources  $\Theta = [\Theta_1, \Theta_2, \dots, \Theta_{24}]^T$  describe the magnetic voltages through the air gap. With  $q = 2$  each complete mesh in the circuit shown in Figure 2 describes a single pole of one phase. The magnetic currents shown can be summarized to

$$\phi = [\phi_1, \phi_{\sigma,1}, \phi_2, \phi_{\sigma,2}, \dots, \phi_{24}, \phi_{\sigma,24}]^T. \quad (1)$$

Using Kirchhoff's first circuit law, the magnetic fluxes per pole can be defined as

$$\phi_{\text{pole}} = [\phi_1 + \phi_{\sigma,1} + \phi_{24} + \phi_{\sigma,24}, \phi_1 + \phi_{\sigma,1} + \phi_2 + \phi_{\sigma,2}, \dots, \phi_{23} + \phi_{\sigma,23} + \phi_{24} + \phi_{\sigma,24}]^T \quad (2)$$

or rearranged in matrix form with a matrix  $T \in \mathbb{R}^{12 \times 24}$



second circuit law for the electric circuit, and Faraday's law of induction, the currents in Equation (10) can be replaced, which then leads to

$$\mathbf{A}_{\text{mag}}(\mathbf{s}, \boldsymbol{\phi}) \boldsymbol{\phi} = \mathbf{T}^T \left( \mathbf{N} \mathbf{R}_{\text{el}}^{-1} \begin{bmatrix} U_1 \\ U_2 \\ U_3 \end{bmatrix} - \begin{bmatrix} \mathbf{n}_1^T \\ \mathbf{n}_2^T \\ \mathbf{n}_3^T \end{bmatrix} \boldsymbol{\phi}_{\text{pole}} \right), \quad (11)$$

with  $[\mathbf{n}_1, \mathbf{n}_2, \mathbf{n}_3]^T$  representing the three columns of  $\mathbf{N}$ . After re-ordering, this results in an IDE in semi-implicit form

$$\mathbf{T}^T \left( \mathbf{N} \mathbf{R}_{\text{el}}^{-1} \begin{bmatrix} \mathbf{n}_1^T \\ \mathbf{n}_2^T \\ \mathbf{n}_3^T \end{bmatrix} \mathbf{T} \right) \boldsymbol{\phi} = \mathbf{T}^T \mathbf{N} \mathbf{R}_{\text{el}}^{-1} \begin{bmatrix} U_1 \\ U_2 \\ U_3 \end{bmatrix} - \mathbf{A}_{\text{mag}}(\mathbf{s}, \boldsymbol{\phi}) \boldsymbol{\phi}. \quad (12)$$

Handling IDEs is not an easy task. Therefore, using a transformation presented in Schmid et al.<sup>11</sup> this IDE is transformed into a differential algebraic equation (DAE)

$$\begin{bmatrix} \dot{\eta}_1 \\ \dot{\eta}_2 \\ \dot{\eta}_3 \end{bmatrix} = \mathbf{R}_{\text{el}}^{-1} \begin{bmatrix} U_1 \\ U_2 \\ U_3 \end{bmatrix} - \mathbf{R}_{\text{el}} \tilde{\mathbf{A}}_{\text{mag}}^{-1}(\mathbf{s}, \boldsymbol{\phi}) \begin{bmatrix} \eta_1 \\ \eta_2 \\ \eta_3 \end{bmatrix}, \quad (13)$$

$$\mathbf{0} = \boldsymbol{\phi} - \mathbf{A}_{\text{mag}}^{-1}(\mathbf{s}, \boldsymbol{\phi}) \mathbf{T}^T \mathbf{N} \tilde{\mathbf{A}}_{\text{mag}}^{-1}(\mathbf{s}, \boldsymbol{\phi}) \mathbf{n} \begin{bmatrix} \eta_1 \\ \eta_2 \\ \eta_3 \end{bmatrix}.$$

The vector  $\boldsymbol{\eta}$  is the time derivative of the introduced auxiliary variable  $\boldsymbol{\eta}$  representing the sum of the pole fluxes per pole pair

$$\begin{aligned} \eta_1 &= \sum_{i \in \mathcal{K}_1} \phi_{\text{pole},i} / \mathcal{K}_1 = \{1, 4, 7, \dots, 22\}, \\ \eta_2 &= \sum_{i \in \mathcal{K}_2} \phi_{\text{pole},i} / \mathcal{K}_2 = \{2, 5, 8, \dots, 23\}, \\ \eta_3 &= \sum_{i \in \mathcal{K}_3} \phi_{\text{pole},i} / \mathcal{K}_3 = \{3, 6, 9, \dots, 24\} \end{aligned} \quad (14)$$

and the invertible matrix is given by  $\tilde{\mathbf{A}}_{\text{mag}}^{-1}(\mathbf{s}, \boldsymbol{\phi}) = \mathbf{N}^T \mathbf{T} \mathbf{A}_{\text{mag}}^{-1}(\mathbf{s}, \boldsymbol{\phi}) \mathbf{T}^T \mathbf{N}$ . Coming back to the structure of the simulation model, the output of the magnet model i.e. the radial magnetomotive force is approximated by

$$F_{\text{magrad},i} = \frac{\mu_{r,\text{Fe}} - 1}{2\mu_{r,\text{Fe}}\mu_0 A_{x,i}} \phi_{\text{Fe},x,i}^2, \quad (15)$$

where the index variable  $x$  describes the different paths of the flux lines.

Using this approach, only the radial magnetomotive forces acting on the rotor are calculated. However, the tangential forces are responsible for the rotation. In a synchronous motor, there is a relationship between the tangential and radial forces. To investigate this relationship, a magnetic FEM simulation of the motor under investigation is made with the aim of applying this relationship to the calculated radial forces. To calculate the magnetic forces in the air gap using FEA, the flux densities

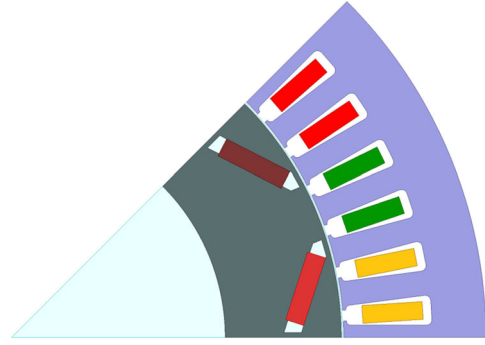


FIGURE 3 Simulated section in the finite element analysis

in the air gap are the starting point. They are calculated in the middle of the air gap. Owing to the symmetry of the motor, it is sufficient to model one pole, which is equal to a section of  $360^\circ/(2p)$  of the machine, with the number of pole pairs  $p$ . This reduced cross-section is shown in Figure 3.

To take further advantage of the symmetry, it is only necessary to simulate the electric period  $T_{\text{el}}$  over one pole pair, which is equal to  $T_{\text{el}}/p$ . Once the simulation is complete, the radial and tangential tensile stress along the air gap can be calculated according to

$$\sigma_{\text{tan}}(x, t) = \frac{B_{\text{rad}}(x, t) \cdot B_{\text{tan}}(x, t)}{\mu_0}, \quad \sigma_{\text{rad}}(x, t) = \frac{B_{\text{rad}}^2(x, t) - B_{\text{tan}}^2(x, t)}{2\mu_0} \quad (16)$$

with the radial  $B_{\text{rad}}$  and tangential  $B_{\text{tan}}$  parts of the flux density.<sup>13</sup> By multiplication with the active length  $l_{\text{Fe}}$  of the machine the stress components are transformed to line loads

$$f_{\text{tan}} = \sigma_{\text{tan}} \cdot l_{\text{Fe}}, \quad f_{\text{rad}} = \sigma_{\text{rad}} \cdot l_{\text{Fe}}. \quad (17)$$

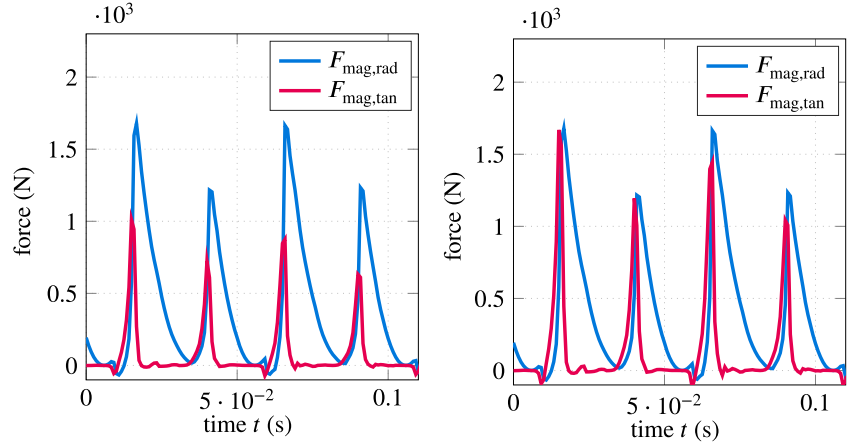
The time-dependent forces for a certain area element followed by multiplying the increment of the discretized air gap circumference  $\Delta x$  with respective to line load component is given as

$$F_{\text{mag,rad/tan}} = f_{\text{rad/tan}} \cdot \Delta x. \quad (18)$$

The primary effort in computing the air gap forces using this approach is the computational time consumed by the FEA simulation.

Figure 4 shows the result of an FEA simulation containing the tangential and radial forces. As mentioned above, there is a relationship between these forces. On the right side of Figure 4, the tangential force is linearly scaled to fit the peaks of the radial forces. The decay behavior can be approximated by a PT1 element but is neglected in this study. As a first approximation, the relationship is thus assumed to be linear and the scaling factor determined in this way is used to estimate the tangential forces from the calculated radial forces.

**FIGURE 4** Relationship between radial and tangential forces from magnetic finite element method simulation (left) and the reasonable scaling for the tangential forces (right)



The calculated magnetomotive forces  $F_{\text{mag,tan}}$  and  $F_{\text{mag,rad}}$  are now fed forward to the mechanical model of the motor.

## 2.2 | Mechanical modeling of the rotor

The rotor is defined as a rigid body including the shaft. At first, all degrees of freedom, except the rotation around the z-coordinate, are locked. The input of the mechanical system is the tangential force vector  $F_{\text{mag,tan}} \in \mathbb{R}^{24 \times 1}$ , the radial force vector  $F_{\text{mag,rad}} \in \mathbb{R}^{24 \times 1}$ , and the load torque  $M_{\text{load}}$ . The frames where the forces act are equally distributed around the rotor's outer radius, depending on the number of stator teeth. In addition to the inputs mentioned, the outputs of the system are the bearing forces occurring at the body's inertial coordinate system and the kinematic states  $\alpha$  and its derivative  $\dot{\alpha}$ . Later, additional mechanical degrees of freedom for rotation around the other axes will be considered for a detailed analysis of bearing forces.

Given the geometry and mass of the rotor and shaft the moments of inertia are calculated. Using this, the equation of motion for this simple system is defined by

$$J\ddot{\alpha} = f - B \cdot u, \quad (19)$$

with  $J$  as the moment of inertia about the center of mass, the acceleration  $\ddot{\alpha}$ , that is the second derivative of the generalized coordinate, and  $f$  the generalized forces. The input vector  $u \in \mathbb{R}^{49 \times 1}$  consists of the stacked load torque, and radial and tangential forces. The vector  $B$  transforms the input forces to the defined application frames of the forces. The mechanical rigid body model is derived and simulated using the software Neweul-M<sup>2</sup>.<sup>9</sup> In Figure 5, the mechanical model is illustrated. The discretely positioned force application frames per stator pole are shown on the sketched cross-section through the rotor as an example. A tangential and radial force  $F_{\text{mag,rad/tan},i}$  acts on each frame around the motor. Also, the body-fixed coordinate system and the acting load torque can be seen.

Since the objective is to study the vibrations that the motor transmits to the housing, the forces that occur in the rotor bearing are calculated in the simulation.

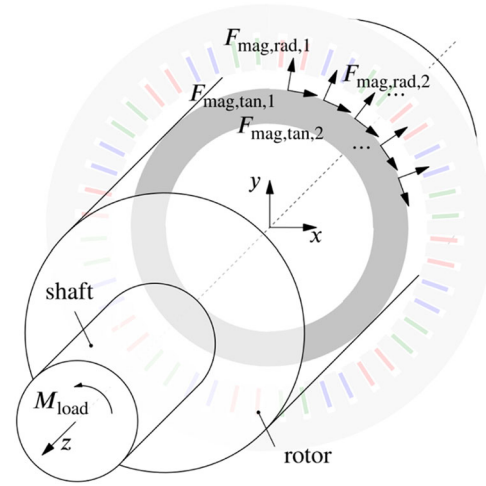


**FIGURE 5** Sketch of the mechanical model with the defined force application points, the body-fixed coordinate system, and the acting load moment

In further investigation, the next step is to replace the rigid body with elastic elements, such as an elastic shaft. An elastic shaft would in turn have an effect on the size of the air gap, which affects the magnetic forces in the gap. Feedback to the magnetic model would then be necessary, but the magnetic model, as described, already uses an air gap that can vary over time, although is assumed to be constant in this first investigation. In addition, it must be considered how the housing is coupled to the motor via the bearings, but this is not a major obstacle using the described force elements. This is close to the goal of dynamically investigating the noise vibration harshness behavior of the engine.

## 3 | EXAMPLE SIMULATION

For the simulations, a CPU with 12 cores and 3.20 GHz is used. For 10 s simulation time, the computational time is approximately 20–30 min. In this example, a constant three-phase alternating current  $U_{\text{inp}}$  is the input of the system, with a peak of 400 V and a

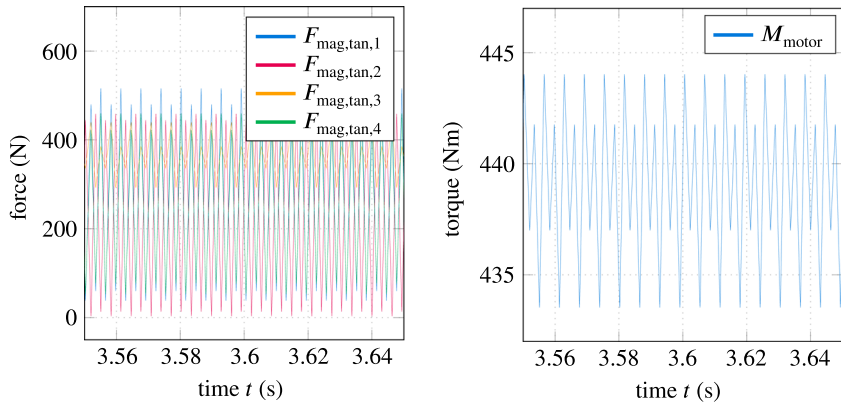


**FIGURE 6** Absolute values of the first four tangential magnetomotive forces  $F_{\text{mag,tan},1-4}$  (left) and the generated torque on the motor  $M_{\text{motor}}$  by all tangential forces without a load torque (right)

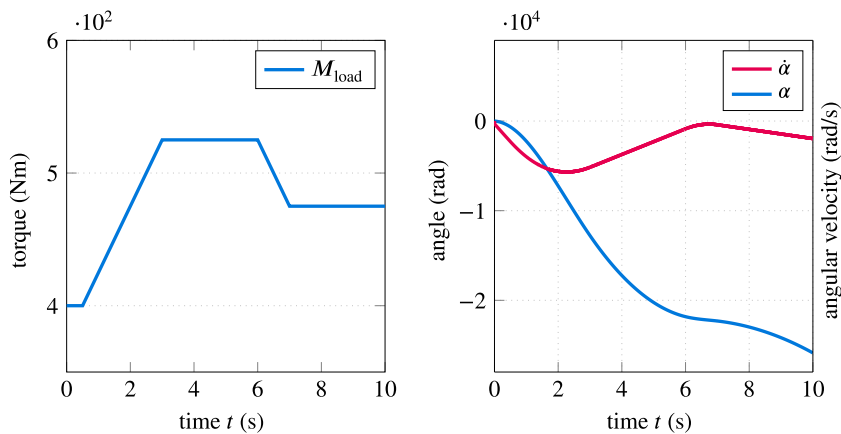


**FIGURE 7** Applied load torque  $M_{\text{load}}$  (left) and resulting mechanical states  $\alpha$  and  $\dot{\alpha}$  (right)

frequency of 1000 rad/s. Figure 6 shows on the left the absolute values of the tangential magnet forces calculated by the simplified magnet model. The magnetomotive force at each magnet is dependent on the material properties and the defined leakage flux through the pole backs. In this first approach, those parameter values are chosen reasonably but will be investigated and adapted in detail later. The magnetic forces always occur in pairs, which means the first 12 are similar to the last 12. Because of the better representability, only the first four are shown, but all 24 forces are in that range. The generated motor torque  $M_{\text{motor}}$ , without the acting load torque, can be seen on the right side of Figure 6. This figure also shows that torque ripples occur, which is a characteristic effect in many electric machines.

The user-defined load torque is varying over time. As shown in Figure 7 on the left, the motor is first operated with a constant load torque of 400 Nm, which then increases after 0.5 s. After 3.5 s, the load torque remains constant again until it decreases at 6 s. Note that the input voltage  $U_{\text{inp}}$  is constant over the whole simulation. On the right of Figure 7, the resulting angle  $\alpha$  and its derivative  $\dot{\alpha}$  are depicted, which describes the rotation of the motor around the z-axis.

The resulting forces on the bearings are calculated afterward. As mentioned, the magnetic forces always occur in pairs on the winding on the opposite sides. Without considering the eccentricity of the rotor or the shaft, there is only one force  $F_y \approx 120\text{ N}$  in the y-direction left, which is the weight force of the rotor and the shaft.

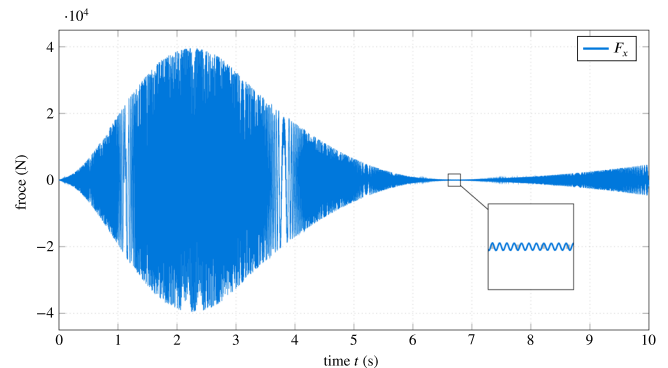


**FIGURE 8** Bearing force in the x-direction that occurs due to the modeled eccentricity

All other forces on the rotor cancel each other out. To show a nonconstant force curve in the bearing, a static eccentricity is now modeled in the rotor. Therefore, the center of gravity of the rotor is shifted by 0.1 mm from the axis of rotation. Since the axis of rotation remains the same, the air gap between rotor and stator also remains constant. Figure 8 shows the resulting force in x-direction on the bearing. As expected, the resulting force is highest when the angular velocity of the rotor is also highest and oscillates at the speed of rotation.

## 4 | CONCLUSION AND OUTLOOK

In this paper, a method was presented to model in a simplified way the electromagnets of a synchronous motor. Starting with an EMC model of the magnets, it is possible to couple the calculated forces that arise in the air gap to a mechanical model. Important effects, such as the magnetic saturation and leakage flux, are not neglected in the process. As result, the magnetomotive forces in the air gap of the motor are the input for a mechanical model. The coupled model allows a very efficient transient simulation and makes an evaluation of the acting forces possible over long times. This type of modeling will by no means replace the detailed magnetic finite element simulation, but for the application of vibration analysis at load changes or changes of the input voltage during operation, this approach could be suitable.

To improve the accuracy of the model, parameter identification is mandatory to validate the model for the specific motor. Therefore, an experiment with the presented motor or a detailed magnetic FEM simulation could be used. The simulation model is modular, which makes it possible to add mechanical or magnetic effects or change the motor design quickly. For example, the magnetic hysteresis, which causes a weakening of the magnetic field during the pole reversal processes, should be implemented during the next steps. In addition, the influence of coupling capacities that occur in the high-frequency range on the magnetic field<sup>14</sup> should be investigated.

On the mechanical side, the next steps are the connection to the housing via force elements representing the bearings and the replacement of the rigid shaft by an elastic shaft. For this step, it is then necessary to implement the feedback to the magnetic model to account for the change in the air gap. Also, other mechanical effects causing vibrations, for example, eccentricity and bearing stiffness can be implemented to investigate and improve the emerging vibrations on the motor.

### ACKNOWLEDGMENTS

The authors would like to express their appreciation to Patrick Schmid for his valuable suggestions and assistance during the development of the magnet model. All authors would like to thank the Ministry of Science, Research, and Arts of the Federal State of Baden-Württemberg for the financial support of the ReMos project “Effiziente Reluktanzmaschine für emissionsfreie Mobilität ohne seltene Erden” within the “InnovationsCampus Mobilität der Zukunft.”

### CONFLICT OF INTEREST

The authors declare that there are no conflict of interest.

### DATA AVAILABILITY STATEMENT

Research data are not shared.

### ORCID

Peter Eberhard  <http://orcid.org/0000-0003-1809-4407>

## REFERENCES

1. Widmer JD, Martin R, Kimiabeigi M. Electric vehicle traction motors without rare earth magnets. *Sustain Mater Technol*. 2015; 3:7-13.
2. Seok-Myeong J, Han-Wook C, Sung-Ho L, Hyun-Sup Y, Yeon-Ho J. The influence of magnetization pattern on the rotor losses of permanent magnet high-speed machines. *IEEE Trans Magn*. 2004;40(4): 2062-2064.
3. Ozcelik NG, Dogru UE, Imeryuz M, Ergene LT. Synchronous reluctance motor vs. induction motor at low-power industrial applications: design and comparison. *Energies*. 2019;12(11):2190.
4. Langheck A, Reuter S, Saburow O, Maertens R, Wittemann F, Berg LF, Doppelbauer M. Evaluation of an integral injection molded housing for high power density synchronous machines with concentrated single-tooth winding. In *Proceedings of the International Electric Drives Production Conference (EDPC)*; 2018:1-6.
5. Schiefer M, Doppelbauer M. Indirect slot cooling for high-power-density machines with concentrated winding. In *Proceedings of the IEEE International Electric Machines Drives Conference (IEMDC)*; 2015: 1820-1825.
6. Maroufian SS, Pillay P. Design and analysis of a novel PM-assisted synchronous reluctance machine topology with AlNiCo magnets. *IEEE Trans Ind Appl*. 2019;55(5):4733-4742.
7. dos Santos FLM, Anthonis J, Naclerio F, Gyselinck JJC, van der Auweraer H, Góes LCS. Multiphysics NVH modeling: simulation of a switched reluctance motor for an electric vehicle. *IEEE Trans Ind Electron*. 2014;61(1):469-476.
8. Kemmetmüller W, Faustner D, Kugi A. Modeling of a permanent magnet synchronous machine with internal magnets using magnetic equivalent circuits. *IEEE Trans Magn*. 2014;50(6):1-14.
9. Kurz T, Eberhard P, Henninger C, Schiehlen W. From Neweul to Neweul-M<sup>2</sup>: symbolical equations of motion for multibody system analysis and synthesis. *Multibody Syst Dyn*. 2010;24(1):25-41.
10. Schiehlen W, Eberhard P. *Applied Dynamics*. Springer; 2014.
11. Schmid P, Schneider G, Dignath F, Liang X, Eberhard P. Static and Dynamic modeling of the electromagnets of the Maglev vehicle transrapid. *IEEE Trans Magn*. 2021;57(2):1-15.
12. Polinder H, Sloopweg J, Hoeijmakers M, Compter J. Modelling of a linear PM machine including magnetic saturation and end effects: maximum force to current ratio. In *Proceedings of the IEEE Int Electric Machines Drives Conference*; 2003;2:805-811.
13. Veeh C. Verein Deutscher Ingenieure & Leibniz Universität Hannover - Institut für Antriebssysteme und Leistungselektronik Oberwellenorientierte Wicklungsmodifikation von permanentmagneterregten Synchronmaschinen mit Zahnspulenwicklung. *Fortschritt-Berichte VDI/ 21: VDI-Verlag*. 2013.
14. Kallenbach E, Eick R, Ströhla T, Feindt K, Kallenbach M, Radler O. *Elektromagnete—Grundlage, Berechnung, Entwurf und Anwendung*. 5th ed. Springer Vieweg; 2017.

**How to cite this article:** Bechler F, Kesten J, Wittemann F, Henning F, Doppelbauer M, Eberhard P. Simplified modeling of electromagnets for dynamic simulation of transient effects for a synchronous electric motor. *Int J Mech Syst Dyn*. 2021;1: 89-95. <https://doi.org/10.1002/msd2.12005>